Simultaneous and rapid removal of Safranin O (SO) and Basic blue 41 (BB) dyes by sulfonated polyacrylamide (PAA-SO3H) as super-adsorbent, isotherms, and kinetics studies

Mohammad Ali Zare (M.A.Zare@miau.ac.ir)
Islamic Azad University Marvdasht https://orcid.org/0000-0003-0655-6440
Zahra Jamali
Islamic Azad University Marvdasht
Abdulhamid Fadavi
Islamic Azad University Marvdasht
Reza Sanaye
Shiraz University of Medical Sciences
Ehsan Vafa
Islamic Azad University Marvdasht
Maryam Iranpour
Islamic Azad University Shiraz

Research Article

Keywords: Super-Adsorbent, Safranin O, Basic blue 41, Removal, Isotherm models, Kinetic models

Posted Date: June 6th, 2022

DOI: https://doi.org/10.21203/rs.3.rs-174770/v2

Simultaneous and rapid removal of Safranin O (SO) and Basic blue 41 (BB) dyes by sulfonated polyacrylamide (PAA-SO_3H) as super-adsorbent, isotherms, and kinetics studies

Mohammad Ali Zare [a]* ● Zahra Jamali[a] ● Abdulhamid Fadavi[a] ● Reza Sanaye[b] ● Ehsan Vafa[c], Maryam Iranpour[d]

[a] Department of Chemistry, Marvdasht Branch, Islamic Azad University, Marvdasht, Iran.

[b] Department of Medical Nanotechnology, School of Advanced and Technologies, Shiraz University of Medical Sciences.

[c] Department of Materials Science and Engineering, Marvdasht Branch, Islamic Azad University, Marvdasht, Iran.

[d] Department of Chemistry, Shiraz Branch, Islamic Azad University, Shiraz, Iran.

*Corresponding author. E-mail: M.A.Zare@miau.ac.ir

Abstract

As a result of their environmental importance, dyes are now one of the most pressing environmental issues. Sulfonated polyacrylamide has been synthesized and fully described, applying FTIR technique. The goal would be delving into the nature of simultaneous ultrasound removal of SO and BB dyes. It could lead to an efficient super-adsorbent for industrial dye processing. Optimization of parameters was conducted using central composite design (CCD) with response surface methodology (RSM). The pH value of 7.9, contact time of 2 minutes, adsorbent dose of 0.008 g, and SO and BB concentrations of 362.02 and 420.45 mg/L were found to be the optimal conditions for dye removal. Adsorption is an ideal approach method for preserving dyes from aqueous industrial wastes because of high efficiency, cost-effectiveness and simplicity. An acceptable degree of consonance between experimental and calculated values was arrived at. High percentage removal (90.01% and 99.95%) of SO and BB in short time (2.16 min) were recorded through the application of an ultrasound-assisted adsorbent (0.008g). Freundlich model shows the proper agreement with the experimental data of both dyes, and the maximum adsorption capacities were *20000* and *8334.0* mg/g for SO and BB, respectively.

Keywords: Super-Adsorbent; Safranin O; Basic blue 41; Removal; Isotherm models; Kinetic models

1. Introduction

There is a relatively wide spectrum of differing pollutants affecting life, of which the two main sources are environmental pollution and human pollution. One of the most significant sources of environmental pollution is sewage coming from industries such as textiles, leather, cytology, printing, food etc.; these apply pigments and dyes in the manufacturing of their final products. The rest of the dyes have the capability to interfere with aquatic life and even to contaminate the food chain. Furthermore, the greater part of the harm arises from the fact that some dyes cause allergy, skin disturbance, irritation, cancer, and even mutation in humans [1]. Consequently, dyes undoubtedly represent a genuine danger not only to water environment but also human health [2]. This is because such dyes possess characteristics of persistent, extremely visible, non-

biodegradable nature; this is over and above the fact that they are mostly stable to oxidizing agent and sunlight [3–5]. Thence, the necessity for the dye-containing water is to undergo treatment prior to any disposal to the environment [4].

It has been estimated that something more than 700,000 t of dyestuff produced per year, in addition to the very available dyes are emitted into the environment while no truly proper treatment has been exerted on them [6]. As a result, there is real necessity to remove these from industrial effluents for purposes of creating a healthy purified aqueous environment. It ought to be noted that the said dyes have some structural diversity—their removal is laborious during the waste water treatment.

In order to eliminate pollutants from wastewater, adsorbents can be introduced as an efficacious and simple method. Several materials such as agricultural wastes, natural compounds, activated carbon, etc. may be made use of as adsorbents. For the simple fact that contaminants are generally removed in an in-discriminant manner, there are many problematic as for selective recovering of the same contaminants to reuse them. Those adsorbents which are produced on the basis of cheap materials are, of course, attractive with many practical applications. Nonetheless, there is immense need to expand the improvement of adsorption capacities, mechanical strength, uncomplicated designing, flexibility, ease of operation [5, 7, 8].

Adsorbents that have polymeric shapes have appeared as sort of a potential remedy to commonly traditional adsorbents. Their efficiency manifests itself as for huge surface area, fully mechanical stiffness, controlled variable surface chemistry, pore size distribution, and feasible regeneration on the basis of mild states [9].

Design according to a methodology of experiential platform causes the evaluating over the main and the combination (interaction) influences on the part of variables in minimum states of experiments [10].

The synthesis of sulfonated polyacrylamide was followed by its characterization by means of FTIR techniques. The SO and BB retrieval from solutions was remarkably accelerated as ultrasonic instrument was brought in to rapidly assist the adsorption method. This was detected by ultraviolet–visible (UV-Vis) spectrophotometer. Next to the pH optimization, the time period of sonicating and initial SO and BB concentrations in addition to the dosage of adsorbent were all examined and actually improved through

the medium of CCD with RSM. The data gained experimentally were fitted to conventional kinetic modeling, including pseudo first and second-order besides intra-particle diffusion models, and so the adsorption was assayed.

2. Experimental

2.1. Instruments and reagents

5.00 mg of each solid dyes of BB and SO in 0.1 L double distilled water were dissolved and the stock solution (0.5 g/L) of them were prepared and the needed concentrations daily were produced by their proper dilution.

The pH measurements were performed by pH meter (Metrohm, model 827, Switzerland) and the BB and SO concentrations were measured by Uv-Vis spectrophotometer (Perkin-Elmer, Lambda 45, USA) and a glass cell with an optical part (1.000 cm at wavelengths of 664.7 and 520.0 nm for BB and SO, respectively). An ultrasonic instrument (model LBS2) at frequency 40 KHz and 285W was used for the ultrasound- adsorption procedure. pH Effect on the performance of adsorption was studied between pHs 2-10. pH of dyes was maintained by 0.1 F Sodium hydroxide and Hydrochloric acid solution.

2.2. Ultrasound- adsorption method

It is possible for the ultrasound to eliminate SO and BB both at the same time. Not only this, but that the ultrasound device also has the capacity to speed up these presses of elimination. All during the experiment, the ultrasound's temperature was kept constant. The experiments as for adsorption were also carried out inside a flask of 50 mL SO and BB solutions with the caveat that 400 mg L^{-1} of both dyes were present. Subsequent to the sonication for 3.0 min with the presence of 0.001 g PAA-SO_3H, the solution went under centrifugation so that the remaining concentrations of both dyes could be examined through the assistance of UV-Vis spectrophotometer with their maximal wavelength of 520.0 nm for SO and 664.7 nm for BB.

2.3. Synthesis of sulfonated polyacrylamide (PAA-SO_3H)

In a 200 mL round-bottom flask, 5.00 g Acryl Amide (70 mmol), 5.17 g 2-acrylamido-2-methylpropansulfonic acid (AAMP) (25 mmol) and 0.77 g N,N`-methylenebisacrylamide (NNMBA) (5 mmol) were dissolved in approximately 100 mL ethanol. 125 mg Benzoyl peroxide (0.5 mmol) was added to them and the mixture was heated while stirring at reflux state for 5 h. Using filtration, the resulted polymer was collected and washed three times with hot ethanol and dried at 70 °C under reduced pressure overnight. Dried polymer weight was 10.10 g which is 91.8% gravimetric yields (Schematic 1). Back titration method also showed a 1.1 mmol/g polymer acidic capacity. This is equivalent to 91% titrimetric yield [11].

2.4. Dye uptake measurements

The concentrations of dye were measured based on the plots of calibration achieved at the equal conditions. The removal percentage (RE%) values of BB and SO were determined using the following Equation (1):

$$RE\% = ((C_0 - C_e)/C_0) \times 100 \quad (1)$$

where, C_0 (mg/L) and C_t (mg/L) are the target concentrations at initial and next time t, respectively. The adsorbed BB and SO amounts (q_e (mg/g)) were calculated as follows:

$$q_e = (C_0 - C_e)V/W \quad (2)$$

where, C_0 and C_e (mg/L) are the initial and equilibrium dye concentrations in aqua, respectively, V (L) is the solution volume and W (g) is the adsorbent mass.

3. Result and discussion

3.1. Characterization of PAA- SO_3H

Fig. 1 shows the FTIR (KBr) spectrum of the PAA-SO_3H adsorbent of SO and BB and adsorbed SO and BB on PAA- SO3H samples. FTIR spectra of the prepared PAA-SO3H adsorbent is presented in Fig. 1a and 1d. Absorption peaks around 3536-3182 cm^{-1} indicates the N–H stretching mode of amino groups. The peak at 1682 cm^{-1} indicates the C=O stretching vibration in amide groups. Peaks at 1444 cm^{-1} and 1182 cm^{-1} and 1038 cm^{-1} indicates the S=O stretching vibration in sulfonate groups. For the BB Fig. 1b, the peak at 3486 cm^{-1} indicates the OH stretching vibration. The peak at 2375 cm^{-1} shows the N=N stretching vibration in azo group. The peak at 1569 cm^{-1} shows the C=N stretching vibration. Following the adsorption of BB onto PAA-SO_3H, two new peaks were seen in 2358 and 1596 cm^{-1} (Fig. 1c), which can be simultaneous with the absorption of BB. Therefore, BB has been anchored on the surface of PAA-SO_3H structures when the adsorption process is carrying out. Absorption peaks around 3536-3182 cm^{-1} shows the N–H stretching mode of amino groups. The peak at 1682 cm^{-1} indicates the C=O stretching vibration in amide groups. Peaks at 1444 cm^{-1} and 1182 cm^{-1} and 1038 cm^{-1} shows the S=O stretching vibration in sulfonate groups. The peak for the SO Fig. 1e at 3330 cm^{-1} indicates the OH stretching vibration. The peak at 2368 cm^{-1} shows the N=N stretching vibration in azo group. Peaks at 1334 cm^{-1} and 1194 cm^{-1} and 1016 cm^{-1} shows the S=O stretching vibration in sulfonate groups. Following the adsorption of SO onto PAA-SO_3H, two new peaks were observed in 2378 and 1522 cm^{-1} (Fig. 1f), which can be during the absorption of SO. Therefore, SO was fixed on the surface of PAA-SO_3H structures when the adsorption process was carrying out [12–14].

PAA-SO_3H has a BET surface area of 64 m^2g^{-1} and a BJH average pore width of 12–18 nm. SEM images, Fig. 2, reveal the morphology and microstructure of PAA-SO_3H, displaying nanosized particles of near sphere or elongated sphere. The EDX scanning, on the other hand, revealed the presence of nitrogen, oxygen, and sulfide contents.

3.2. Central Composite Design (CCD

In a central composite design, the methodology is, in point of fact, a statistical one under the title of RSM: this method applies experimental data for the pure purpose of modeling and optimizing any kind of processes where our intended response might in any way be under the influence of multiple variables. The mathematical techniques used

here in RSM comprise of a number of experimental designs dependent on the very important issue of response prediction. The real point of RSM would thus turn out to be hypothesizing over the empirical fitting of predictions to the obtained data. Here we are taking about Five parameters:

Initial SO concentration (X_1), and initial BB concentration (X_2), pH (X_3), PAA-SO_3H mass (X_4), Contact time (X_5).

According to our CCD approach, optimization was overall necessary in order to arrive at the best optimal response(s). As a result, five different levels were assigned to parameters, each consisting of −α, −1, 0, +1, and +α, which are shown in Table 1 as the lowest, low, center, high, and highest levels, respectively. The design matrix and the responses are presented in Table 2.

The adequacy of the model arises from estimating coefficients to predict responses pertaining to each of the abovementioned factors. Each single experimental run has to be compared with the other four factors according to the polynomial quadratic equation as follows:

$$y = \beta_0 + \sum_{i=1}^{3} \beta_i \chi_i + \sum_{i=1}^{3} \sum_{j=1}^{3} \beta_{ij} \chi_i \chi_j + \sum_{i=1}^{3} \beta_{ii} \chi_i^2 \qquad (3)$$

where Xi's are the independent variables while y would be the predicted response.

RSM's advantage over other methodologies is that, response variation is able to be clearly visualized through 3D response surface.

Significant parameters within the model are specified by p-Value and F-Value. Here p-Value has a level of p=0.05 such that dose parameters whose value is less than 0.05 are deemed significant. It is also to be noted that any higher F-value implies (more) accurate predicting for experimental data. In fact, the signal-to-noise-ratio here is the revealed precision ratio of predicted values to the average predicted errors. It is to be mentioned that variance coefficient and adequate are 0.41 and 105.65 (for SO), 0.36 and 154.28 (for BB), respectively. Worthy of attention is that the quality of curve-fitting is determined by determination coefficient (R^2) and the adjusted coefficient of determination (R^2 adj.). When these two parameters are close to 1, the model fitting will become of even greater importance. Accordingly, the R^2 of (0.999) and the R^2 adj. of (0.998) reveal that the numerical values predicted by RSM are thus quite close to those obtained throughout experiments.

The significantly important interactions in our work include the following:

X_1, X_2, X_3, X_4, X_5, X_1X_2, X_1X_3, X_1X_4, X_1X_5, X_2X_3, X_2X_4, X_2X_5, X_3X_4, X_3X_5, X_4X_5, X_1^2, X_2^2, X_3^2, X_4^2, X_5^2

It turns out to be true that significant interactions appear with a positive sign in the prediction formulae while interactions that are insignificant reveal themselves with a negative sign in the formulae:

$$R\%SO = +759.29 -2.45X_1 -1.34X_2 +54.66X_3 -18509.54X_4 +13.92X_5 +3.93E\text{-}3X_1X_2 +0.020X_1X_3 +70.61X_1X_4 +0.06X_1X_5 -0.05X_2X_3 +9.08X_2X_4 -0.03X_2X_5 -2440.99X_3X_4 -2.49X_3X_5 -1249.48X_4X_5 -3.24E\text{-}4X_1^2 +6.41E\text{-}5X_2^2 -0.46X_3^2 +3.12E+5X_4^2 +0.88X_5^2 \quad (4)$$

$$R\%BB = +881.62 -2.06X_1 -1.76X_2 +69.47X_3 -35715.79X_4 -41.20X_5 +2.37E\text{-}3X_1X_2 -0.038X_1X_3 +79.06X_1X_4 +0.091X_1X_5 -0.052X_2X_3 +34.81X_2X_4 +0.031X_2X_5 -1189.12X_3X_4 -2.61X_3X_5 +425.51X_4X_5 +2.77E\text{-}4X_1^2 +8.001E\text{-}4X_2^2 -0.80X_3^2 -1.17E+5X_4^2 +0.80X_5^2 \quad (5)$$

where R% SO and R% BB represent the responses, the percentage of the SO and SO mixing dyes adsorption in the solution is indicated. In general, when each parameter's coefficient is strong, it confirm that the answer is highly positive. However, the negative value of each parameter indicates a reversed association between the reactions and the parameter, such that the negative value leads to maximum reactions.

The optimum values (Fig. 3) for factors such as the adsorbent quantity, pH, SO concentration, BB concentration, and contact time were obtained as 0.008, 7.9, 360.62, 420.29 and 2.16, respectively. Under such circumstances, removal percentage for SO and BB was predicted to be 90.05% and 99.86% respectively with 0.999 desirability. Quick adsorption was observed for both responses in a matter of 2.16 minutes. It was understood form the curves that time had had no great effect on the dyes' removal percentage. In fact, the highest level of adsorption had taken place early in the process. This means that the availability of many sites earlier in the process and their decrease later on, could have led to decrease in adsorption levels. The very high levels of adsorption speed for PAA-SO_3H might as well give us great hope for many more applications of PAA-SO_3H in the future. It was also observed that with the increase in the adsorbent levels, the removal percentage of both dyes would well increase [15–17]. This can be related to the adsorbent surface increase. It can also be related to more availability of a greater number of sites for adsorption.

It is to be noted that the adsorption percentage does decrease with an increase in the primary concentration of the dye: this is the results of the saturation of adsorption sites. High levels of adsorption in earlier higher concentrations are the result of coming into force of some “push” to overcome the dye’s mass transmission between the aqueous phase and the solid phase [18, 19]. As could be seen, under circumstances of LOW pH’s, removal percentage is LOW: this phenomenon has arisen from H^+ ions’ competition with various species of dyes over adsorption sites. As the pH increases, the adsorption level increases, too. Zero-point charge (ZPC) is an important term to detect the pH at which the material's surface has a number of loaded functions which is positive and negative. Therefore, the adsorbent surface becomes even more negative (in view of pH_{zpc} = 7.6), leading to the adsorption of dyes with positive charges through the means of electrostatic force (onto the adsorbent surface). The three-dimensional (3D) diagrams of the effect of different parameters on the removal of SO and BB are shown in Figure 4.

750

3.3. Study of equilibrium absorption isotherms

Isotherm models are used to provide an insight into the absorption mechanism, surface properties, adsorbent tendency, and descriptions of absorption experimental data. Several adsorption equilibrium isotherms that are widely used to analyze equilibrium data of solute between adsorbent and solution in solid systems are Langmuir, Freundlich, Tempkin and Deboning–Radushkevich (D–R) isotherms. These isotherm models were used to fit the experimental data in the present study.

3.4. The Langmuir isotherm

This isotherm [20] is widely used for modeling equilibrium data. The Langmuir model was assumed that sorption occurs in a monolayer, surface is homogeneous and there is no interaction between adjacent adsorbed molecules. In this model, the linear equation is represented by the following equation:

$$C_c/q_e = 1/K_a Q_m + C_e/Q_m \quad (6)$$

The linear plots of C_e/q_e versus C_e suggest the applicability of the Langmuir isotherm in Table 4. The correlation coefficients reported in the Table 4 demonstrated powerful positive evidence on the adsorption of the SO and BB onto the PAA-SO_3H using the Langmuir model.

3.5. The Freundlich isotherm

One of the most common models to describe adsorption isotherms is the Freundlich isotherm [21]. This model describes a reversible adsorption of multilayers of adsorbed molecules in a heterogeneous system. The well-known linear form of the Freundlich isotherm is represented by the empirical equation:

$$Lnq_e = LnK_f + (1/n)LnC_e \quad (7)$$

here, q_e is the amount of the adsorption SO and BB (mg/g), C_e is the equilibrium concentration of SO and BB in the solution (mg/L). K_f and 1/n are the Freundlich equilibrium and adsorption constant, respectively. K_f indicative of adsorption capacity of PAA-SO_3H and 1/n show adsorption intensity in Table 4. The reasonable correlation coefficients (0.988–0.993 for PAA-SO_3H) indicates its higher efficiency for the interpretation of experimental data than the Langmuir isotherm. 1/n value changes when the mass of adsorbent from 0.539 to 0.475 raised. The K_f has increased with adsorbent mass from 145.525 to 232.273. It indicates that the adsorption capacity of the adsorbent raised in a unit equilibrium concentration for adsorption of more species.

3.6. The Tempkin isotherm

Another empirical equation that studies the absorption processes is the Tempkin model. This isotherm expresses the adsorption mechanism with an adsorbent– adsorbate interaction. The isotherm is given by the following equations Equation (8) [22]:

$$q_e = RT/b\, LnAC_e \quad (8)$$

This isotherm was simplified as follows [23, 24]:

$$q_e = \beta Ln\alpha + \beta LnC_e \quad (9)$$

R= Ideal gas constant (8.314 J/(mol/K))

b_T= Temkin isotherm constant

β=Constant related to heat of sorption (J/mol)

T= Temperature at 298K.

When the experimental equilibrium data were fitted to the above-mentioned equation revealed the high and reasonable applicability of this isotherm to interpret and explain the SO and BB adsorption onto PAA- SO_3H in Table 4.

3.7. The Deboning–Radushkevich (D–R) isotherm

A useful empirical theory that express the adsorption mechanism with a Gaussian energy distribution onto a heterogeneous surface is D–R isotherm [25, 26]. The non-linear and linear equation can be illustrated Equation (10) and Equation (11) respectively:

$$q_e = Q_m \exp\left(-K\varepsilon^2\right) \quad (10)$$

$$Lnq_e = LnQ_m - K\varepsilon^2 \quad (11)$$

where, Q_m is the theoretical saturation capacity K_{DR} ($mol^2/(KJ^2)$) is related to free energy of adsorption and ε is the Polanyi potential that can represented by Equation (12):

$$\varepsilon = RTLn\left(1 + 1/C_e\right) \quad (12)$$

Based on Equation (10), plotting Ln q_e versus ε^2 enables to be determine as K ($mol^2/(kJ)^2$) and adsorption capacity (Q_m (mg/g)) through the interception and the slope values, respectively.

The K gives the mean free energy (E) of sorption per molecule of the sorbate from infinity in solution to the solid surface can be illustrated as Equation (13) [27]

$$E = 1/\sqrt{2K} \quad (13)$$

The estimated values of D–R parameters are given in Table 4 The model saturation adsorption capacity at optimum states by adsorbents in the range of 0.008–0.01 g, respectively has proper agreement with the relative Langmuir value (20000.0 for SO and 8333.0 mg/g for BB).

3.8. Adsorption kinetics

In this study, several Kinetic models and their parameters have been used to describe and predict adsorption data and potential rate controlling steps, which are helpful for the prediction of adsorption rate, describe the kinetic process of adsorption and give important information for designing and modeling the adsorption processes. Here we used four widely-used kinetic models to investigate the processes of the simultaneous adsorption of SO and BB on the PAA-SO_3H. Therefore, the mentioned models are discussed in the following sections.

The rate of adsorption in pseudo-first-order model [28] is based on the adsorption capacity and generally expressed as follows Equation (14):

$$Ln\left(q_e - q_t\right) = Lnq_e - K_1 t \quad (14)$$

where, q_e and q_t are the amount of the SO and BB on the PAA-SO_3H surface at equilibrium and at time t (mg/g), respectively. k_1 is the pseudo-first order rate constant (L/min). By this equation, the plot of first order model log (q_e -q_t) versus t for the adsorption of SO and BB concentration on the PAA-SO_3H C_0= 350.0 (mg/L) at 25^0C show that the correlation coefficient (R^2) for each dye is 0.918 and 0.924, respectively and comparatively low for most adsorption data and another concentration (C_0= 450.0 (mg/L)). Therefore, the reaction mechanism for adsorption of SO and BB on the PAA-SO_3H surface is inappropriate. Then, kinetic data are fitted with another model [22, 29]. The adsorption kinetic can be described by the pseudo-second order model [30] and may be expressed in the form:

$$t/q_t = 1/K_2 q_e^2 + t/q_e \quad (15)$$

The curve fitting plot of log (q_e - q_t) versus t does not show good results for the entire adsorption period. The kinetic data such as k_2 and equilibrium adsorption capacity, q_e, for the adsorption of SO and BB onto PAA-SO_3H surface were calculated based on the intercept and slope of the plot of t/q_t versus t, respectively in Table 5. The values of correlation coefficients R^2, is closer to unity (0.999) for the pseudo-second-order kinetic model for all initial dye concentrations (350.0 mg/L and 450.0 mg/L), as presented in Table 5. This shows that the adsorption mechanism of PAA-SO_3H obeys the pseudo-second-order kinetic model for the entire adsorption period. Also, with increasing initial concentration SO and BB, the diffusion rate enhancement and the value of k_2 increased.

One of the most useful kinetic model to evaluate the adsorption process is the Elovich equation [22]. This equation is expressed as follows according to the adsorption capacity:

$$q_t = 1/\beta\, Ln(t) + 1/\beta\, Ln(\alpha\beta) \quad (16)$$

Important parameters, such as Elovich maximum adsorption capacity and Elovich constant can be calculated from the slope and intercept of the equation of Equation (16) and reported in Table 5.

Another kinetic model that evaluate the adsorption process is Intra-particle diffusion [31, 32]. In this process, SO and BB may be transported and movement from the bulk of the solution to the adsorbent (PAA-SO_3H) by intra-particle diffusion. Therefore, the intraparticle diffusion model has been used to study the rate-limiting step for the adsorption of both dyes onto PAA- SO_3H surface. A general equation indicates the intra-particle diffusion model as follows:

$$q_t = K_{id} t^{1/2} + C \quad (17)$$

The values of k_{id} and C are determined using the slope and intercept of the plot of q_t versus $t^{1/2}$, respectively in Table 5. C and k_{id} are constant and intra particle diffusion rate constant, respectively. If the plot of q_t versus $t^{1/2}$ passes through the origin, intra-particle diffusion alone is the rate limiting step [33]. Based on the obtained data in Table 5, The R^2 value for this kinetic model was far from the unity. This show that the intra-particle diffusion model cannot be appropriate. As a final result and R^2 values obtained, we concluded that pseudo-second-order kinetic model for the SO and BB removal over entire sorption period is understood [34].

Table 6 compares several reported adsorbents for dyes removal from aqueous solutions. The adsorption capacity of dyes onto PAA-SO_3H is higher than or comparable with previously reported adsorbents.

4. Conclusions

The synthesis of PAA-SO_3H had been carried out and used as a novel adsorbent to rapid individually and simultaneously adsorb of SO and BB. The optimum and best condition for the factors of pH, adsorbent dose, SO and BB concentrations and contact time were 7.90, 0.008g, 360.62 and 420.29 mg/L and 2.16 min, respectively. At this state, the removal percentage of SO and BB calculated by 99.9%. A quick adsorption process (2.16 min) using PAA-SO_3H is so expected for important adsorption usages. An empirical explanation of a competitive Freundlich model was proposed to calculate the simultaneous adsorption of SO and BB. Four Conventional kinetic models were used, and it seems that pseudo-second order equation is proper for fitting the empirical data. It is shown that the pseudo-second-order model has proper fitting with the adsorption data for both dyes. Several isotherm models were investigated to explain the experimental data and their parameters, and also correlation coefficients were determined.

Freundlich model shows the proper agreement with the experimental data of both dyes, and the maximum adsorption capacities were *20000.0* and *8333.0* mg/g for SO and BB, respectively.

References

1. Mullerova S, Baldikova E, Prochazkova J, et al (2019) Magnetically modified macroalgae Cymopolia barbata biomass as an adsorbent for safranin O removal. Mater Chem Phys 225:174–180
2. An Y, Zheng H, Yu Z, et al (2020) Functioned hollow glass microsphere as a self-floating adsorbent: Rapid and high-efficient removal of anionic dye. J Hazard Mater 381:120971
3. Regti A, Laamari MR, Stiriba S-E, El Haddad M (2017) Removal of Basic Blue 41 dyes using Persea americana-activated carbon prepared by phosphoric acid action. Int J Ind Chem 8:187–195
4. Mahmoodi NM, Abdi J (2019) Nanoporous metal-organic framework (MOF-199): Synthesis, characterization and photocatalytic degradation of Basic Blue 41. Microchem J 144:436–442
5. Tan TCN, Sen TK (2020) Aqueous-phase methylene blue (MB) dye removal by mixture of eucalyptus bark (EB) biomass and kaolin clay (KC) adsorbents: kinetics, thermodynamics, and isotherm modeling. Sep Sci Technol 55:1036–1050
6. Shariati S, Faraji M, Yamini Y, Rajabi AA (2011) Fe3O4 magnetic nanoparticles modified with sodium dodecyl sulfate for removal of safranin O dye from aqueous solutions. Desalination 270:160–165 . doi: https://doi.org/10.1016/j.desal.2010.11.040
7. Noroozi B, Sorial GA (2013) Applicable models for multi-component adsorption of dyes: A review. J Environ Sci 25:419–429 . doi: https://doi.org/10.1016/S1001-0742(12)60194-6
8. Mahmoodi NM (2011) Equilibrium, Kinetics, and Thermodynamics of Dye Removal Using Alginate in Binary Systems. J Chem Eng Data 56:2802–2811 . doi: 10.1021/je101276x

9. Pan B, Pan B, Zhang W, et al (2009) Development of polymeric and polymer-based hybrid adsorbents for pollutants removal from waters. Chem Eng J 151:19–29 . doi: https://doi.org/10.1016/j.cej.2009.02.036

10. Pizarro C, Sáenz-González C, Pérez-del-Notario N, González-Sáiz JM (2012) Development of an ultrasound-assisted emulsification–microextraction method for the determination of the main compounds causing cork taint in wines. J Chromatogr A 1229:63–71 . doi: https://doi.org/10.1016/j.chroma.2012.01.033

11. Khodadoust S, Hadjmohammadi M (2011) Determination of N-methylcarbamate insecticides in water samples using dispersive liquid–liquid microextraction and HPLC with the aid of experimental design and desirability function. Anal Chim Acta 699:113–119 . doi: https://doi.org/10.1016/j.aca.2011.04.011

12. Li F, Bao Y, Chai J, et al (2010) Synthesis and Application of Widely Soluble Graphene Sheets. Langmuir 26:12314–12320 . doi: 10.1021/la101534n

13. Deng S, Li X, Fu H (2011) Acid violet 6B as a novel corrosion inhibitor for cold rolled steel in hydrochloric acid solution. Corros Sci 53:760–768 . doi: http://dx.doi.org/10.1016/j.corsci.2010.11.002

14. Koohi AD, Moghaddam AZ, Sefti MV, Moghadam AM (2011) Swelling and gelation time behavior of sulfonated polyacrylamide/chromium triacetate hydrogels. J Macromol Sci Part B 50:1905–1920

15. Al-Ghouti MA, Al-Absi RS (2020) Mechanistic understanding of the adsorption and thermodynamic aspects of cationic methylene blue dye onto cellulosic olive stones biomass from wastewater. Sci Rep 10:1–18

16. JAFARI MH, Yari AR, Rajabizadeh A, et al (2013) Hazardous and industrial wastes management: A case study of Khazra Industrial Park, Kerman

17. Chikri R, Elhadiri N, Benchanaa M (2020) Efficiency of Sawdust as Low-Cost Adsorbent for Dyes Removal. J Chem 2020:

18. Rene ER, Shu L, Jegatheesan V (2018) Environmentally friendly (bio) technologies for the removal of emerging organic and inorganic pollutants from water. J Water Supply Res Technol 67:697–702

19. Abuzerr S, Darwish M, Mahvi AH (2018) Simultaneous removal of cationic methylene blue and anionic reactive red 198 dyes using magnetic activated carbon nanoparticles: equilibrium, and kinetics analysis. Water Sci Technol 2017:534–545

20. Langmuir I (1918) The adsorption of gases on plane surfaces of glass, mica and platinum. J Am Chem Soc 40:1361–1403

Freundlich HMF (1906) Over the adsorption in solution. J Phys Chem 57:1100–1107 21.

Aharoni C, Ungarish M (1977) Kinetics of activated chemisorption. Part 2.—Theoretical models. J Chem Soc Faraday Trans 1 Phys Chem Condens Phases 73:456–464 22.

Tempkin MI, Pyzhev V (1940) Kinetics of ammonia synthesis on promoted iron catalyst. Acta Phys Chim USSR 12:327 23.

Akkaya G, Özer A (2005) Biosorption of Acid Red 274 (AR 274) on Dicranella varia: Determination of equilibrium and kinetic model parameters. Process Biochem 40:3559–3568 . doi: https://doi.org/10.1016/j.procbio.2005.03.048 24.

Dubinin MM (1965) Modern state of the theory of volume filling of micropore adsorbents during adsorption of gases and steams on carbon adsorbents. Zhurnal Fiz Khimii 39:1305–1317 25.

Dubinin Mm (1960) The potential theory of adsorption of gases and vapors for adsorbents with energetically nonuniform surfaces. Chem Rev 60:235–241 26.

Radushkevich L V (1949) SORBTSIYA I STRUKTURA AKTIVNYKH UGLEI. 7. POTENTSIALNAYA TEORIYA ADSORBTSII I STRUKTURA AKTIVNYKH UGLEI. ZHURNAL Fiz KHIMII 23:1410–1420 27.

LAGERGREN, S. (1898) Zur theorie der sogenannten adsorption geloster stoffe. K Sven Vetenskapsakademiens Handl 24:1–39 28.

Weber WJ, Morris JC (1963) Kinetics of adsorption on carbon from solution. J Sanit Eng Div 89:31–60 29.

Ho YS, McKay G (1999) Pseudo-second order model for sorption processes. Process Biochem 34:451–465 . doi: https://doi.org/10.1016/S0032-9592(98)00112-5 30.

Thompson LH, Doraiswamy LK (1999) Sonochemistry: Science and Engineering. Ind Eng Chem Res 38:1215–1249 . doi: 10.1021/ie9804172 31.

Chakma S, Moholkar VS (2011) Mechanistic features of ultrasonic desorption of aromatic pollutants. Chem Eng J 175:356–367 . doi: https://doi.org/10.1016/j.cej.2011.09.123 32.

Midathana VR, Moholkar VS (2009) Mechanistic Studies in Ultrasound-Assisted Adsorption for Removal of Aromatic Pollutants. Ind Eng Chem Res 48:7368–7377 . doi: 10.1021/ie900049e 33.

Maddikeri GL, Pandit AB, Gogate PR (2012) Adsorptive Removal of Saturated and Unsaturated Fatty Acids Using Ion-Exchange Resins. Ind Eng Chem Res 51:6869– 34.

6876 . doi: 10.1021/ie3000562

35. Behboudi G, Shayesteh K, Yaraki MT, et al (2021) Optimized synthesis of lignin sulfonate nanoparticles by solvent shifting method and their application for adsorptive removal of dye pollutant. Chemosphere 285:131576

36. Abukhadra MR, El-Meligy MA, El-Sherbeeny AM (2020) Evaluation and characterization of Egyptian ferruginous kaolinite as adsorbent and heterogeneous catalyst for effective removal of safranin-O cationic dye from water. Arab J Geosci 13:169

37. Vidovix TB, Quesada HB, Bergamasco R, et al (2021) Adsorption of Safranin-O dye by copper oxide nanoparticles synthesized from Punica granatum leaf extract. Environ Technol 1–17

38. Sharifpour E, Ghaedi M, Nasiri Azad F, et al (2018) Zinc oxide nanorod-loaded activated carbon for ultrasound-assisted adsorption of safranin O: Central composite design and genetic algorithm optimization. Appl Organomet Chem 32:e4099

39. Januário EFD, Vidovix TB, de Araújo LA, et al (2021) Investigation of Citrus reticulata peels as an efficient and low-cost adsorbent for the removal of safranin orange dye. Environ Technol 1–37

40. Azimvand J, Didehban K, Mirshokraie SA (2018) Safranin-O removal from aqueous solutions using lignin nanoparticle-g-polyacrylic acid adsorbent: Synthesis, properties, and application. Adsorpt Sci Technol 36:1422–1440

41. Shelar-Lohar G, Joshi S (2019) Amidoximated functionalized sodium alginate graft copolymer: An effective adsorbent for rapid removal of cationic dyes. Mater Today Proc

42. Ghosh I, Kar S, Chatterjee T, et al (2021) Adsorptive removal of Safranin-O dye from aqueous medium using coconut coir and its acid-treated forms: Adsorption study, scale-up design, MPR and GA-ANN modeling. Sustain Chem Pharm 19:100374

43. Sewu DD, Woo SH, Lee DS (2021) Biochar from the co-pyrolysis of Saccharina japonica and goethite as an adsorbent for basic blue 41 removal from aqueous solution. Sci Total Environ 797:149160

44. Kul AR, Aldemir A, Koyuncu H (2021) An investigation of natural and modified diatomite performance for adsorption of Basic Blue 41: isotherm, kinetic, and

thermodynamic studies. Desalin WATER Treat 229:384–394

45. Gougazeh M, Kooli F, Buhl J-C (2019) Removal Efficiency of Basic Blue 41 by Three Zeolites Prepared from Natural Jordanian Kaolin. Clays Clay Miner 67:143–153

46. Afshin S, Mokhtari SA, Vosoughi M, et al (2018) Data of adsorption of Basic Blue 41 dye from aqueous solutions by activated carbon prepared from filamentous algae. Data Br 21:1008–1013

47. Pushpa T B, Josephraj J, Saravanan P, Ravindran G (2019) Biodecolorization of Basic Blue 41 using EM based Composts: Isotherm and Kinetics. ChemistrySelect 4:10006–10012

48. Kooli F, Liu Y, Abboudi M, et al (2019) Waste Bricks Applied as Removal Agent of Basic Blue 41 from Aqueous Solutions: Base Treatment and Their Regeneration Efficiency. Appl Sci 9:1237

49. Kamaru AA, Sani NS, Malek NANN (2016) Raw and surfactant-modified pineapple leaf as adsorbent for removal of methylene blue and methyl orange from aqueous solution. Desalin Water Treat 57:18836–18850 . doi: 10.1080/19443994.2015.1095122

50. Humelnicu I, Băiceanu A, Ignat M-E, Dulman V (2017) The removal of Basic Blue 41 textile dye from aqueous solution by adsorption onto natural zeolitic tuff: Kinetics and thermodynamics. Process Saf Environ Prot 105:274–287

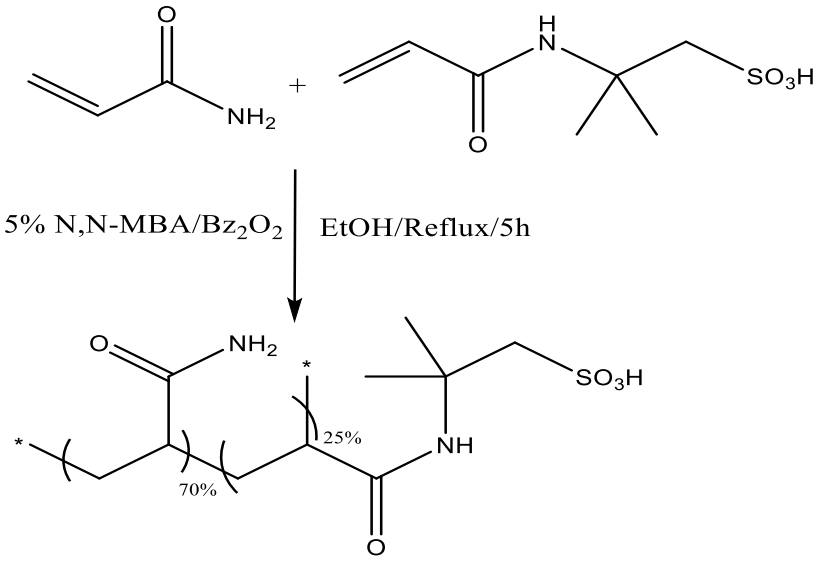

5% Crosslinked Sulfonated polyacrylamide or (PAA-SO_3H)

Schematic 1 Preparation of sulfonated polyacrylamide via transamidation reaction

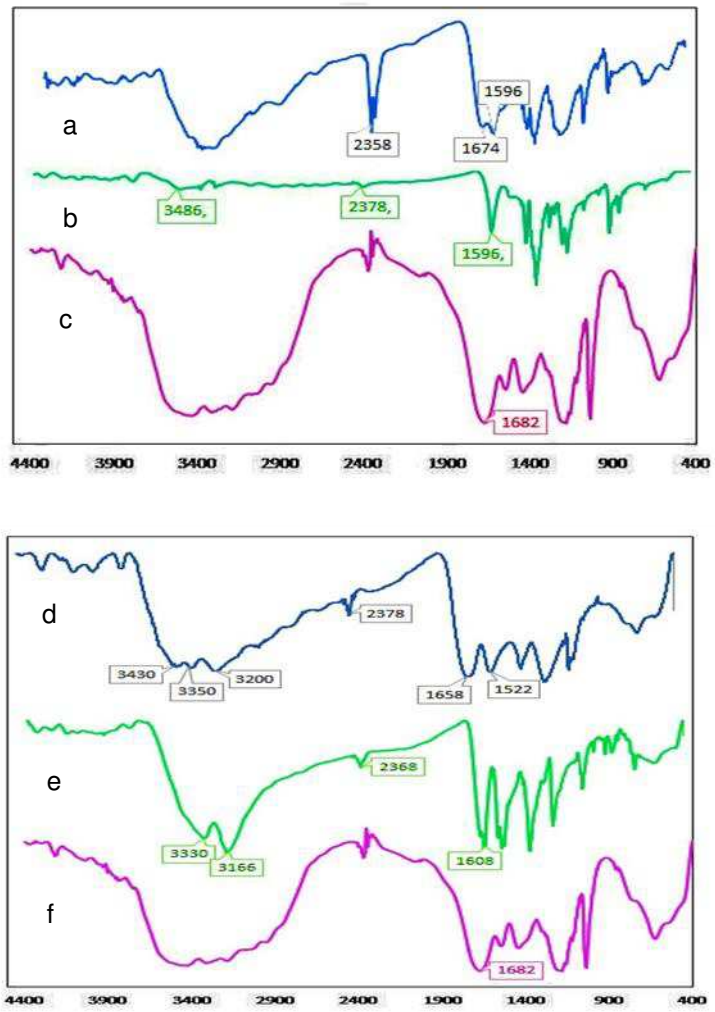

Fig. 1. FT-IR (KBr) for the developed adsorbent. (a) adsorbed BB on PAA- SO_3H (b) BB, (c) PAA- SO_3H adsorbent, (d) adsorbed SO on PAA- SO_3H (e) SO, (f) PAA- SO_3H adsorbent.

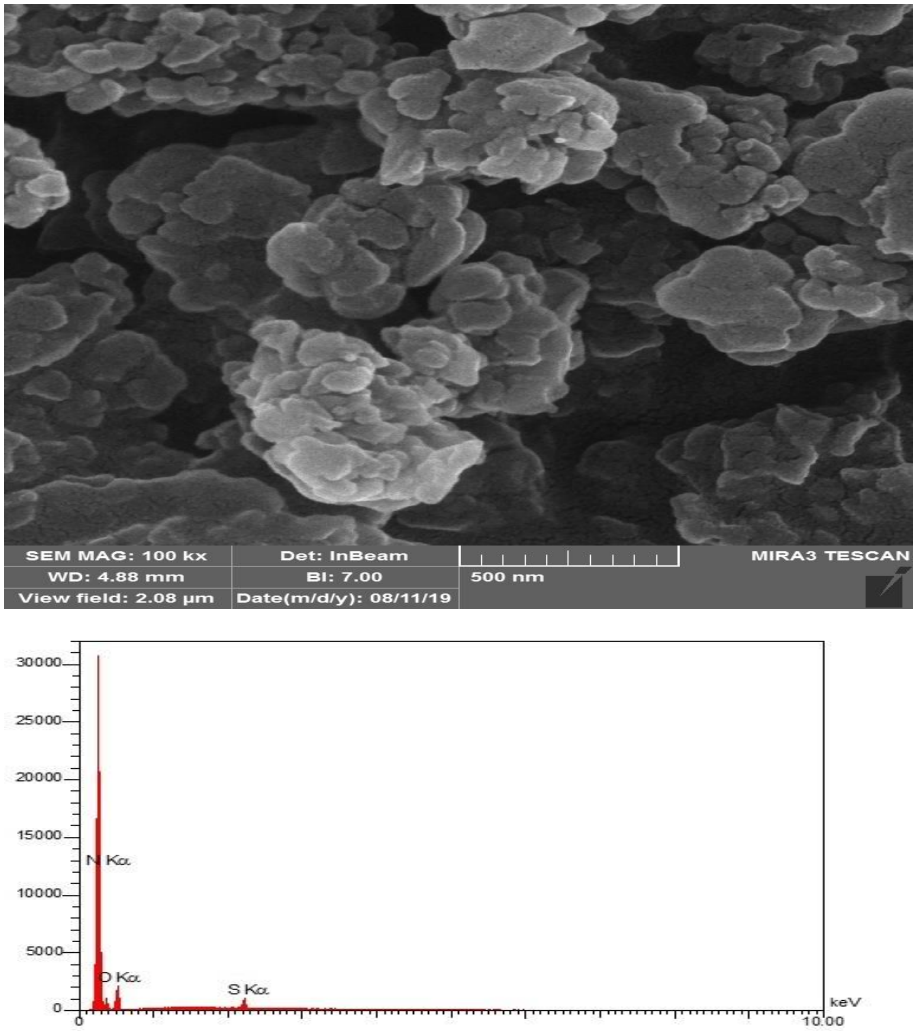

Fig. 2. FE-SEM/EDX analysis of PAA-SO_3H Adsorbent.

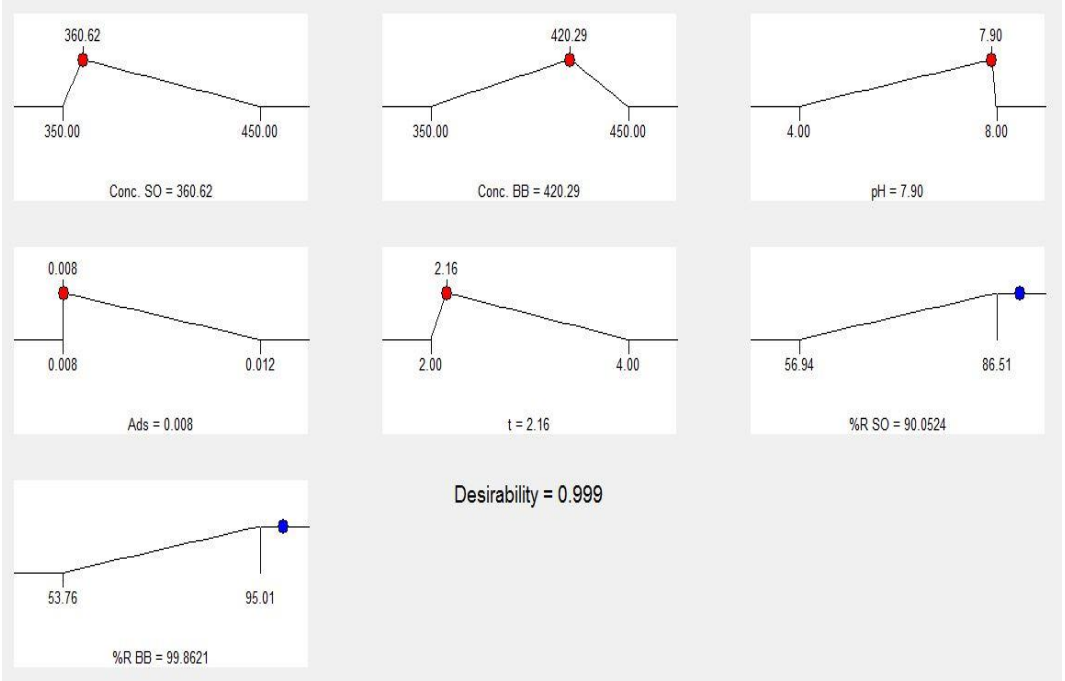

Fig. 3. Optimization plot of factors.

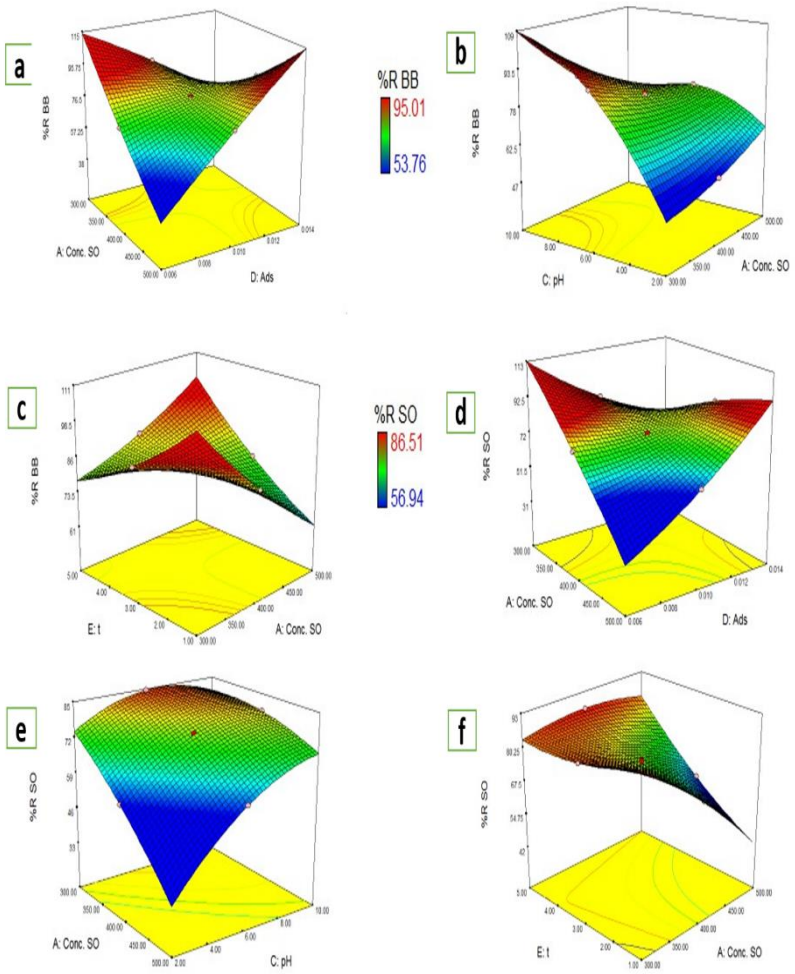

Fig. 4. 3D diagram of SO and BB dyes removal in terms of: conc. SO and PAA-SO3H mass (a), pH and conc. SO (b), time and conc. SO (c), conc.SO and PAA-SO3H mass (d), conc. SO and pH (e), and time and conc. SO (f).

Table 1. The CCD method for removing dyes (SO and BB) from the aqueous environment has operating variables and a functional range.

Variables	Unit	Levels			Star point = 2	
		Low (-1)	Central (0)	High (+1)	-α	+α
(X_1) SO concentrations	mgL^{-1}	350.0	400.0	450.0	300.0	500.0
(X_2) BB concentrations	mgL^{-1}	350.0	400.0	450.0	300.0	500.0
(X_3) pH	_	4.00	6.00	8.00	2.00	10.00
(X_4) adsorbent amount	g	0.008	0.01	0.012	0.006	0.014
(X_5) sonication time	min	2	3	4	1	5

Table 2. Experimental conditions and values obtained through the CCD.

Runs	X_1	X_2	X_3	X_4	X_5	%RE SO	%RE BB
1	400.0	400.0	6.00	0.010	5.00	86.51	87.01
2	400.0	400.0	6.00	0.010	3.00	74.81	82.19
3	400.0	400.0	6.00	0.010	3.00	75.11	81.81
4	350.0	350.0	8.00	0.012	4.00	82.69	87.62
5	400.0	400.0	2.00	0.010	3.00	56.94	53.76
6	500.0	400.0	6.00	0.010	3.00	59.44	78.42
7	400.0	400.0	6.00	0.010	1.00	70.97	83.05
8	450.0	350.0	8.00	0.012	2.00	72.65	87.62
9	450.0	450.0	4.00	0.008	4.00	66.28	75.42
10	400.0	400.0	6.00	0.010	3.00	75.59	81.29
11	300.0	400.0	6.00	0.010	3.00	84.49	90.71
12	450.0	350.0	4.00	0.012	4.00	78.21	77.65
13	350.0	450.0	4.00	0.012	4.00	78.22	88.75
14	350.0	350.0	4.00	0.008	2.00	70.87	80.67
15	400.0	400.0	6.00	0.010	3.00	75.61	81.95

16	450.0	450.0	8.00	0.008	2.00	73.62	69.54
17	400.0	400.0	6.00	0.014	3.00	85.15	86.45
18	400.0	400.0	6.00	0.010	3.00	75.11	81.86
19	350.0	450.0	8.00	0.008	4.00	76.21	80.31
20	400.0	300.0	6.00	0.010	3.00	81.96	95.01
21	450.0	450.0	4.00	0.012	2.00	85.89	89.62
22	350.0	450.0	8.00	0.012	2.00	60.89	82.88
23	400.0	400.0	6.00	0.006	3.00	75.29	73.39
24	400.0	500.0	6.00	0.010	3.00	69.75	84.58
25	400.0	400.0	10.00	0.010	3.00	78.66	84.25
26	450.0	350.0	8.00	0.008	4.00	82.12	79.22

Table 3. Variance analysis for the removal of dyes (%R).

Variance analysis for the removal of SO (%R)						Variance analysis for the removal of BB (%R)				
Source	Sum of Squares	df	Mean Square	F Value	P value (Prob>F)	Sum of Squares	df	Mean Square	F Value	P value (Prob>F)
Model	1549.5	20	77.48	777.67	< 0.0001	1583.0	20	79.15	894.25	< 0.0001
X_1	314.00	1	314.00	3151.73	< 0.0001	75.52	1	75.52	853.28	< 0.0001
X_2	74.54	1	74.54	748.20	< 0.0001	54.39	1	54.39	614.55	< 0.0001
X_3	235.88	1	235.88	2367.59	< 0.0001	464.82	1	464.82	5251.71	< 0.0001
X_4	48.61	1	48.61	487.91	< 0.0001	85.28	1	85.28	963.55	< 0.0001
X_5	120.75	1	120.75	1211.96	< 0.0001	7.84	1	7.84	88.59	0.0002
X_1X_2	328.00	1	328.00	3292.28	< 0.0001	119.06	1	119.06	1345.19	< 0.0001
X_1X_3	13.61	1	13.61	136.60	< 0.0001	50.36	1	50.36	568.95	< 0.0001
X_1X_4	169.03	1	169.03	1696.65	< 0.0001	211.91	1	211.91	2394.27	< 0.0001
X_1X_5	32.71	1	32.71	328.30	< 0.0001	69.60	1	69.60	786.41	< 0.0001
X_2X_3	107.33	1	107.33	1077.28	< 0.0001	92.79	1	92.79	1048.34	< 0.0001
X_2X_4	2.80	1	2.80	28.09	0.0032	41.08	1	41.08	464.16	< 0.0001
X_2X_5	8.56	1	8.56	85.92	0.0002	8.29	1	8.29	93.64	0.0002
X_3X_4	323.22	1	323.22	3244.22	< 0.0001	76.70	1	76.70	866.61	< 0.0001
X_3X_5	84.47	1	84.47	847.84	< 0.0001	92.52	1	92.52	1045.34	< 0.0001
X_4X_5	21.17	1	21.17	212.51	< 0.0001	2.46	1	2.46	27.74	0.0033
X_1^2	17.99	1	17.99	180.54	< 0.0001	13.13	1	13.13	148.40	< 0.0001
X_2^2	0.70	1	0.70	7.06	0.0450	109.47	1	109.47	1236.86	< 0.0001

X_3^2	93.97	1	93.97	943.20	< 0.0001	279.63	1	279.63	3159.36	< 0.0001
X_4^2	42.86	1	42.86	430.18	< 0.0001	6.00	1	6.00	67.80	0.0004
X_5^2	21.26	1	21.26	213.44	< 0.0001	17.91	1	17.91	202.37	< 0.0001
Residual	0.50	5	0.100			0.44	5	0.089		
Lack of Fit	6.1E-3	1	6.1E-3	0.050	0.8341	6.1E-3	1	6.1E-3	0.056	0.8241
Pure Error	0.49	4	0.12			0.44	4	0.11		
Cor. Total	1550.05	25				1583.4	25			

Table 4. Isotherm constant of SO and BB on PAA-SO_3H at optimum condition.

Isotherm	Parameters	Adsorbent (g)			
		0.008		0.01	
		SO	BB	SO	BB
Langmuir	Q_m (mg/g)	20000.0	8333.0	1111.2	5263.2
	K_a (L/mg)	0.0096	0.00012	0.0012	0.0067
	R^2	0.988	0.9646	0.826	0.985
Freundlich	1/n	0.78	0.5398	0.782	0.475
	K_F (L/mg)	302.0	154.5	32.2	232.2
	R^2	0.995	0.988	0.991	0.993
Tempkin	B_1	3246.2	1828.3	1761.1	1205
	K_T (L/mg)	7.04	40.4	57.7	16.5
	R^2	0.991	0.968	0.962	0.983
D-R	Q_s (mg/g)	6272.9	4591.6	3245.4	3124.4
	B	-3E-5	-0.0015	0.0018	-0.00035
	E (kJ/mol)	129.0	3.3	16.6	37.8
	R^2	0.908	0.813	0.830	0.860

Table 5. Kinetic parameters of SO adsorption onto PAA- SO_3H (0.008g of adsorbent, 350.0 and 450.0 mg/L for SO to BB concentration ratio at optimum conditions of other variables).

Model	Parameter	Concentration dyes			
		350.0 (mg/L)		450.0 (mg/L)	
		SO	BB	SO	BB
First order kinetic model	K_1	0.931	0.9094	0.956	0.941
	q_e(calc)	195.1	113.7	188.6	118.6
	R^2	0.918	0.924	0.951	0.957
Second order kinetic model	K_2	0.027	0.0428	0.031	0.044
	q_e (calc)	181.8	204.08	222.2	256.4
	h	909.0	1785.71	1550.6	2941.1
	R^2	0.999	0.999	0.999	0.999
Intraparticle diffusion	K_{diff}	54.89	34.65	61.69	46.97
	C	1959.9	2058.3	2510.4	2633.6
	R^2	0.993	0.939	0.899	0.796
Elovich	β	0.0275	0.0437	0.0235	0.0302
	R^2	0.972	0.919	0.954	0.885

Table 6. Comparison of adsorption capacity of different adsorbents for removal SO and BB.

Adsorbents	Adsorbate	Adsorption capacity ($mg.g^{-1}$)	Reference
lignin sulfonate nanoparticles	Safranin O	85.1	[35]
Egyptian ferruginous kaolinite	Safranin O	59.3	[36]
Copper oxide nanoparticles	Safranin O	189.5	[37]
Zinc oxide nanorod-loaded activated carbon	Safranin O	32.06	[38]
Citrus reticulata peels	Safranin O	464	[39]
Lignin nanoparticle	Safranin O	99	[40]
Lignin Nanoparticle-G-Polyacrylic Acid		138.88	
Sodium Alginate Graft Copolymer	Safranin O	23.98	[41]
Coconut coir modified with phosphoric acid	Safranin O	80.32	[42]
PAA-SO_3H	Safranin O	*20000.0*	Present study
Saccharina japonica and goethite	Basic Blue 41	1494	[43]
Mn-modified diatomite	Basic Blue 41	62.5	[44]
Zeolite	Basic Blue 41	39	[45]

Activated carbon prepared from filamentous algae	Basic Blue 41	125	[46]
Effective Microorganisms	Basic Blue 41	456.8	[47]
Waste Bricks	Basic Blue 41	60	[48]
Pineapple leaf	Basic Blue 41	52.6	[49]
Zeolitic tuff	Basic Blue 41	192.31	[50]
PAA-SO_3H	Basic Blue 41	*8333.0*	Present study